Science Advances
AAAS

Supplementary Materials for

Capillary flow control in lateral flow assays via delaminating timers

Dohwan Lee, Tevhide Ozkaya-Ahmadov, Chia-Heng Chu, Mert Boya,
Ruxiu Liu, A. Fatih Sarioglu*

*Corresponding author. Email: sarioglu@gatech.edu

Published 1 October 2021, *Sci. Adv.* **7**, eabf9833 (2021)
DOI: 10.1126/sciadv.abf9833

The PDF file includes:

Figs. S1 to S10
Legends for movies S1 and S2
References

Other Supplementary Material for this manuscript includes the following:

Movies S1 and S2

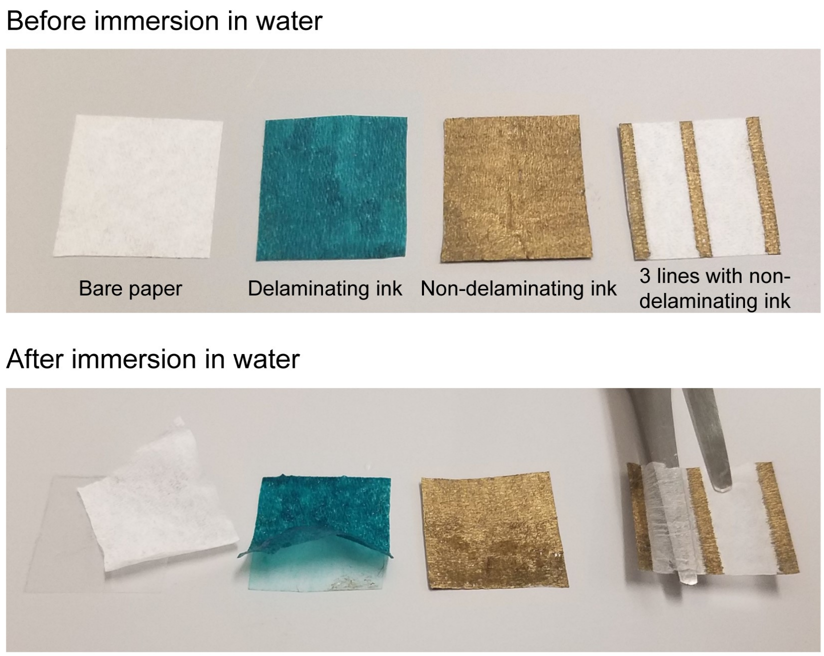

Fig. S1. Delamination of laminated papers painted with the delaminating ink and the non-delaminating ink after immersion. Photos show the state of laminated papers after they were immersed in water for the same duration. The bare paper was fully delaminated from the sheath tape. The paper painted with the delaminating ink adhered to the sheath tape pre-immersion but delaminated when wetted. The paper painted with the non-delaminating ink was strongly tethered to the sheath tape even after immersion. For the paper on which three parallel lines were drawn with the non-delaminating ink, only the regions with no paint were delaminated while the lines remained adhered to the sheath tape. Photo Credit: Dohwan Lee, Georgia Institute of Technology.

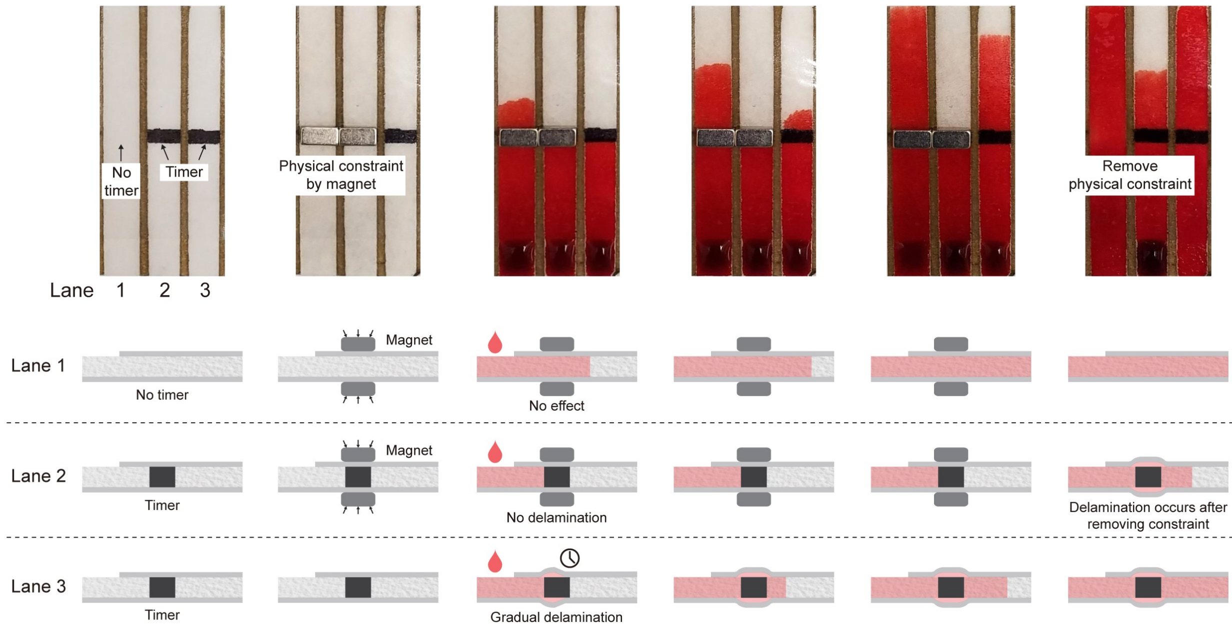

Fig. S2. Investigation of the delay mechanism in delaminating timers. The top photos taken at different time frames show the state of three parallel lanes defined by non-delaminating ink on a laminated paper. Cross-sectional schematics below photos illustrate the corresponding scenarios for each image. In images, lane 1 is a control channel with no timer, while timers were drawn in lanes 2 and 3. Lanes 1 & 2 were first constrained by a mechanical force produced by two attracting magnets. The capillary flow in lane 1 was observed to be unaffected by the mechanical compression. In contrast, the capillary flow in lane 2 stopped permanently. The capillary flow in lane 3 was initially stopped by the timer and resumed after an intended amount of delay. The capillary flow in lane 2 resumed when the physical constraint was removed. Taken together, these results showed the physical separation (i.e., delamination) between the paper and the sheath tape as the mechanism for delaying the capillary flow.

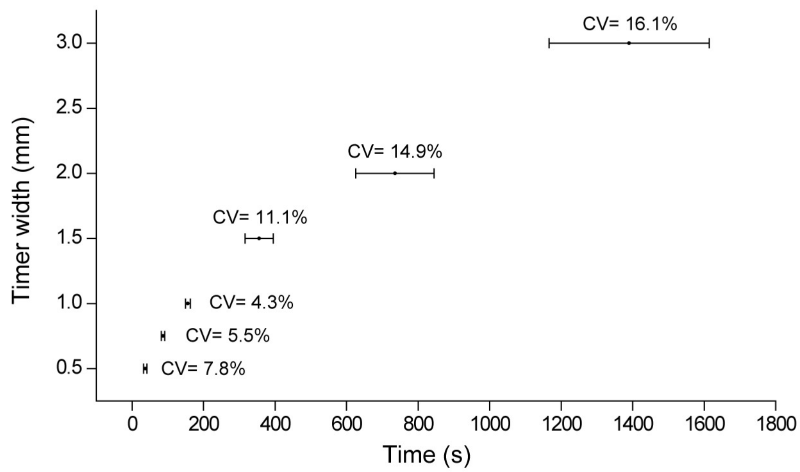

Fig. S3. Characterization of the variation in the time delay produced by delaminating timers. Measured time delays produced by timers as a function of their width. The dots show the mean, the error bars represent the standard deviation (N=10) and CV represents the coefficient of variation.

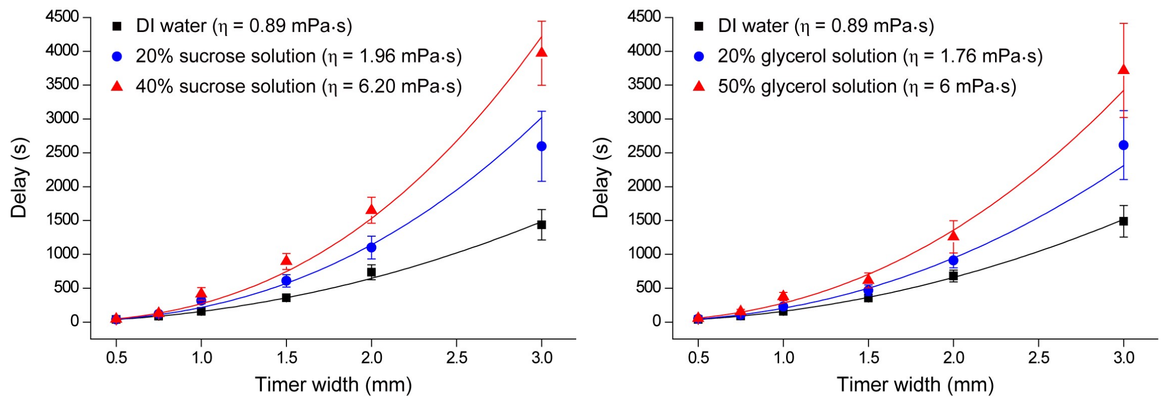

Fig. S4. Effect of liquid viscosity on the timer delay. The plots show the mean measured timer delay as a function of the timer width in response to DI water with its viscosity manipulated by adding sucrose (left) and glycerol (right) at varying concentrations. The expected viscosity values for each tested sample were taken from the literature (*35, 36*) and provided on the plots. The error bars represent standard deviation (N=10).

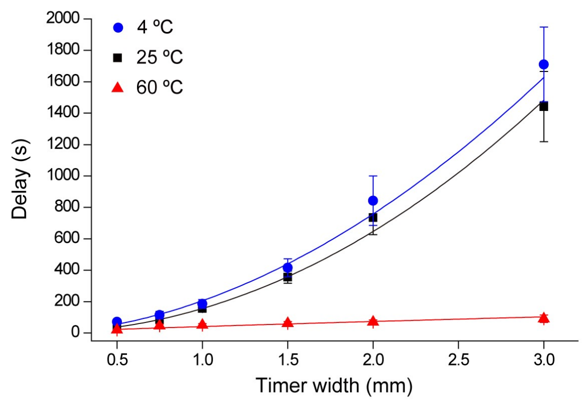

Fig. S5. Effect of temperature on the timer delay. The plot shows the mean measured timer delay as a function of the timer width in response to DI water flow at three different temperatures: 4 °C, room temperature (25 °C), and 60 °C. The external temperature was controlled by a thermoelectric plate. The error bars represent standard deviation (N=10).

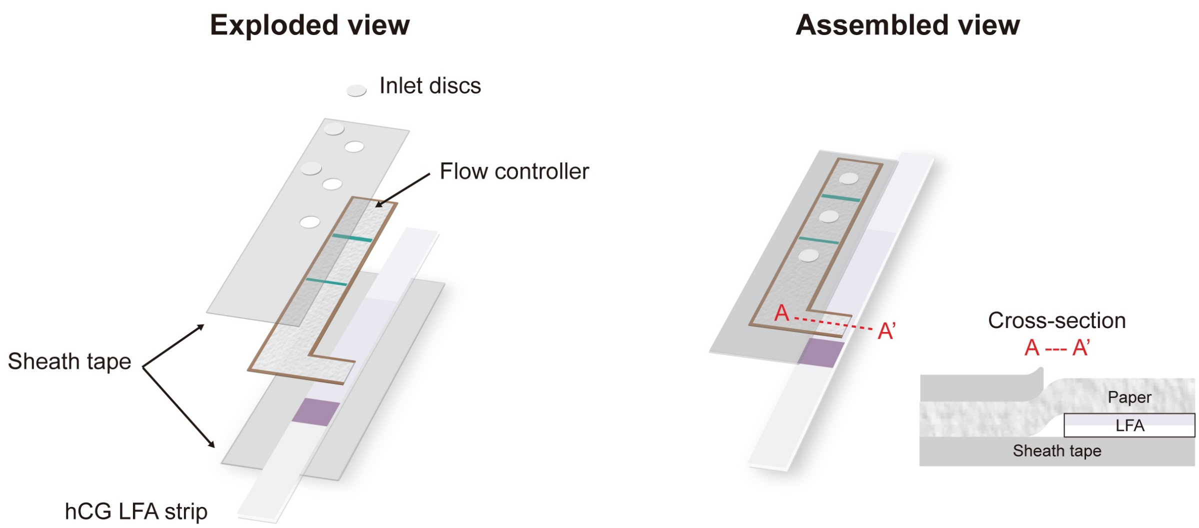

Fig. S6. Integration of the hCG LFA strip with the flow controller. The schematics show the exploded (left) and assembled (right) views of the designed device. The flow controller and commercial LFA strip were aligned and integrated on the same sheath tape at the bottom. Another sheath tape covered the flow controller from the top. To prevent any potential interference with the operation and colorimetric detection, the LFA strip was left exposed from the top with neither the top sheath tape nor the paper substrate extending over the LFA strip except at the junction point that delivers the reagents A/B and DI water from the flow controller to the LFA strip.

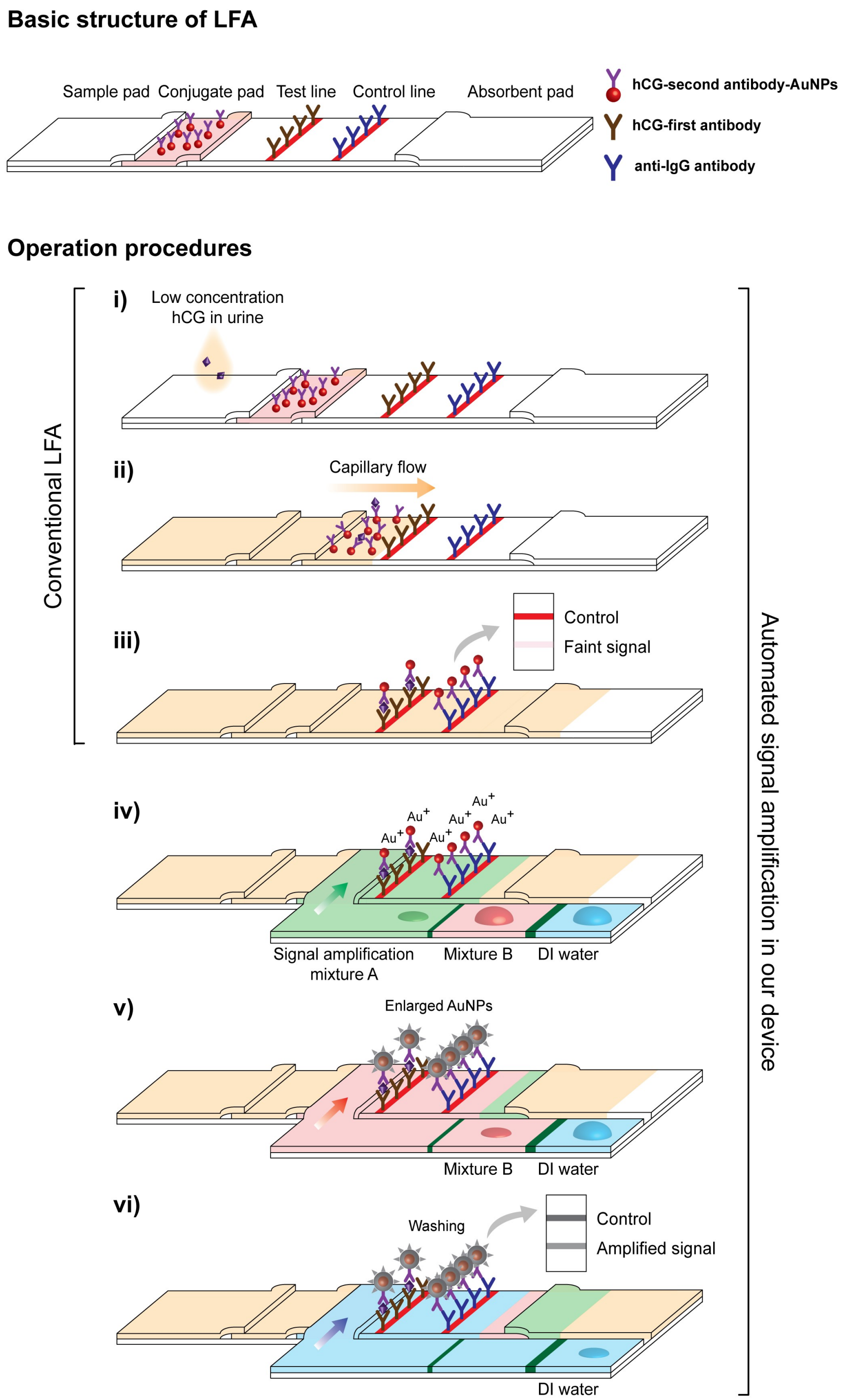

Fig. S7. Operation of the LFA strip with the flow controller. The top schematic shows the basic structure of the conventional LFA indicating the types and placements of bio-recognition elements on the strip. The schematics i-vi show the full sequence of events that produce an amplified colorimetric signal in our device. Among these schematics, i-iii are common with a conventional LFA strip. Schematics iv-vi illustrate the automated signal amplification process through sequential delivery of the chemical reagents by the integrated flow controller.

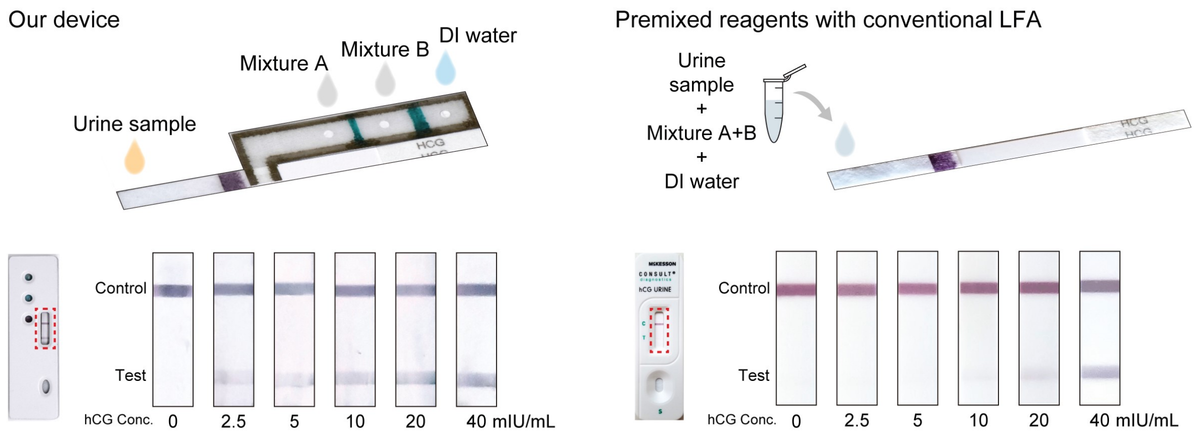

Fig. S8. Comparison between hCG assay on our device and processing the sample premixed with amplification reagents on a conventional LFA. Schematics at the top illustrate the experimental procedures employed to process the urine samples. The urine samples were processed directly on our device, while the samples were premixed with amplification reagents for the conventional LFA. The images below show the colorimetric results recorded from the two experiments for different concentrations of hCG in urine samples. The test line being visible on our device for a lower hCG concentration demonstrates that it is not the presence of amplification reagents but their sequential delivery is responsible for higher sensitivity.

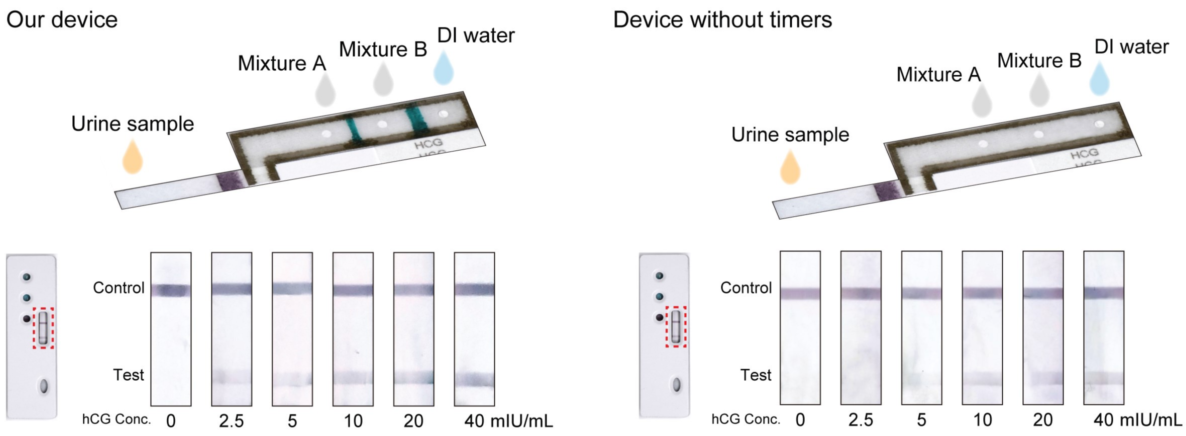

Fig. S9. Comparison between hCG assay on our device and an identical device without delaminating timers. Schematics at the top illustrate the experimental procedures employed to process the urine samples. The only difference between the two devices is that the device on the right does not have the delaminating timers. The images below show the colorimetric results recorded from the two experiments for different concentrations of hCG in urine samples. The test line being visible on our device for a lower hCG concentration demonstrates that the specific time delays produced by delaminating timers are required to increase the assay sensitivity.

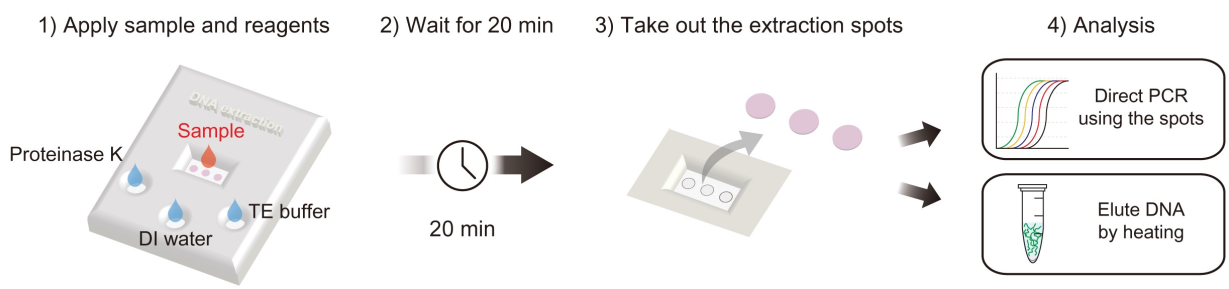

Fig. S10. DNA extraction on our device. The schematic illustrates the steps in the designed protocol. The biological sample is introduced to the device simultaneously with three other reagents from dedicated inlets. After 20 minutes, the extraction spots are taken out from the device and are subjected to PCR for amplification of the extracted DNA. The purified DNA can also be obtained in suspension by immersing the extraction spots in TE or elution buffer and heating at 80 °C for 30 minutes.

Movie S1. Timer response on laminated versus naked paper. The capillary flow was initially stopped by the timer on the laminated paper and then resumed after an intended delay. In contrast, the capillary flow was permanently blocked by an identically-designed timer on a naked paper.

Movie S2. Sequential release of different capillary flow streams with a group of delaminating timers. Four inlets, each with a different number of delaminating timers, merge into a single channel. Differential delays in branches lead to the sequential release of the distinctly colored dye solutions into the main channel. The flow in a similar channel layout without delaminating timers is also shown for comparison purposes.

REFERENCES AND NOTES

1. E. K. Sackmann, A. L. Fulton, D. J. Beebe, The present and future role of microfluidics in biomedical research. *Nature* **507**, 181–189 (2014).
2. M. M. Gong, D. Sinton, Turning the page: Advancing paper-based microfluidics for broad diagnostic application. *Chem. Rev.* **117**, 8447–8480 (2017).
3. A. K. Yetisen, M. S. Akram, C. R. Lowe, Paper-based microfluidic point-of-care diagnostic devices. *Lab Chip* **13**, 2210–2251 (2013).
4. G. A. Posthuma-Trumpie, J. Korf, A. van Amerongen, Lateral flow (immuno)assay: Its strengths, weaknesses, opportunities and threats. A literature survey. *Anal. Bioanal. Chem.* **393**, 569–582 (2009).
5. D. Lee, Y. Shin, S. Chung, K. S. Hwang, D. S. Yoon, J. H. Lee, Simple and highly sensitive molecular diagnosis of Zika virus by lateral flow assays. *Anal. Chem.* **88**, 12272–12278 (2016).
6. R. Banerjee, A. Jaiswal, Recent advances in nanoparticle-based lateral flow immunoassay as a point-of-care diagnostic tool for infectious agents and diseases. *Analyst* **143**, 1970–1996 (2018).
7. T. Kong, S. Flanigan, M. Weinstein, U. Kalwa, C. Legner, S. Pandey, A fast, reconfigurable flow switch for paper microfluidics based on selective wetting of folded paper actuator strips. *Lab Chip* **17**, 3621–3633 (2017).
8. M. S. Verma, M. N. Tsaloglou, T. Sisley, D. Christodouleas, A. Chen, J. Milette, G. M. Whitesides, Sliding-strip microfluidic device enables ELISA on paper. *Biosens. Bioelectron.* **99**, 77–84 (2018).
9. E. Fu, T. Liang, P. Spicar-Mihalic, J. Houghtaling, S. Ramachandran, P. Yager, Two-dimensional paper network format that enables simple multistep assays for use in low-resource settings in the context of malaria antigen detection. *Anal. Chem.* **84**, 4574–4579 (2012).
10. B. J. Toley, B. McKenzie, T. Liang, J. R. Buser, P. Yager, E. Fu, Tunable-delay shunts for paper microfluidic devices. *Anal. Chem.* **85**, 11545–11552 (2013).
11. B. Lutz, T. Liang, E. Fu, S. Ramachandran, P. Kauffman, P. Yager, Dissolvable fluidic time delays for programming multi-step assays in instrument-free paper diagnostics. *Lab Chip* **13**, 2840–2847 (2013).
12. C.-M. Cheng, A. W. Martinez, J. Gong, C. R. Mace, S. T. Phillips, E. Carrilho, K. A. Mirica, G. M. Whitesides, Paper-based ELISA. *Angew. Chem. Int. Ed.* **49**, 4771–4774 (2010).
13. A. W. Martinez, S. T. Phillips, M. J. Butte, G. M. Whitesides, Patterned paper as a platform for inexpensive, low-volume, portable bioassays. *Angew. Chem. Int. Ed.* **46**, 1318–1320 (2007).

14. A. W. Martinez, S. T. Phillips, G. M. Whitesides, Three-dimensional microfluidic devices fabricated in layered paper and tape. *Proc. Natl. Acad. Sci. U.S.A.* **105**, 19606–19611 (2008).
15. Y. Lu, W. Shi, L. Jiang, J. Qin, B. Lin, Rapid prototyping of paper-based microfluidics with wax for low-cost, portable bioassay. *Electrophoresis* **30**, 1497–1500 (2009).
16. Y. Lu, W. Shi, J. Qin, B. Lin, Fabrication and characterization of paper-based microfluidics prepared in nitrocellulose membrane by wax printing. *Anal. Chem.* **82**, 329–335 (2010).
17. D. A. Bruzewicz, M. Reches, G. M. Whitesides, Low-cost printing of poly(dimethylsiloxane) barriers to define microchannels in paper. *Anal. Chem.* **80**, 3387–3392 (2008).
18. X. Li, J. Tian, G. Garnier, W. Shen, Fabrication of paper-based microfluidic sensors by printing. *Colloids Surf. B Biointerfaces* **76**, 564–570 (2010).
19. K. Abe, K. Suzuki, D. Citterio, Inkjet-printed microfluidic multianalyte chemical sensing paper. *Anal. Chem.* **80**, 6928–6934 (2008).
20. K. Abe, K. Kotera, K. Suzuki, D. Citterio, Inkjet-printed paperfluidic immuno-chemical sensing device. *Anal. Bioanal. Chem.* **398**, 885–893 (2010).
21. X. Li, J. Tian, T. Nguyen, W. Shen, Paper-based microfluidic devices by plasma treatment. *Anal. Chem.* **80**, 9131–9134 (2008).
22. X. Li, J. Tian, W. Shen, Progress in patterned paper sizing for fabrication of paper-based microfluidic sensors. *Cellul.* **17**, 649–659 (2010).
23. G. Chitnis, Z. Ding, C. L. Chang, C. A. Savran, B. Ziaie, Laser-treated hydrophobic paper: An inexpensive microfluidic platform. *Lab Chip* **11**, 1161–1165 (2011).
24. K. L. Dornelas, N. Dossi, E. Piccin, A simple method for patterning poly(dimethylsiloxane) barriers in paper using contact-printing with low-cost rubber stamps. *Anal. Chim. Acta* **858**, 82–90 (2015).
25. E. Fu, B. Lutz, P. Kauffman, P. Yager, Controlled reagent transport in disposable 2D paper networks. *Lab Chip* **10**, 918–920 (2010).
26. A. Apilux, Y. Ukita, M. Chikae, O. Chailapakul, Y. Takamura, Development of automated paper-based devices for sequential multistep sandwich enzyme-linked immunosorbent assays using inkjet printing. *Lab Chip* **13**, 126–135 (2013).
27. J. H. Shin, J. Park, S. H. Kim, J. K. Park, Programmed sample delivery on a pressurized paper. *Biomicrofluidics* **8**, 054121 (2014).
28. X. Li, P. Zwanenburg, X. Liu, Magnetic timing valves for fluid control in paper-based microfluidics. *Lab Chip* **13**, 2609–2614 (2013).

29. M. Fratzl, B. S. Chang, S. Oyola-Reynoso, G. Blaire, S. Delshadi, T. Devillers, T. Ward, N. M. Dempsey, J.-F. Bloch, M. M. Thuo, Magnetic two-way valves for paper-based capillary-driven microfluidic devices. *ACS Omega* **3**, 2049–2057 (2018).
30. H. Chen, J. Cogswell, C. Anagnostopoulos, M. Faghri, A fluidic diode, valves, and a sequential-loading circuit fabricated on layered paper. *Lab Chip* **12**, 2909–2913 (2012).
31. B. J. Toley, J. A. Wang, M. Gupta, J. R. Buser, L. K. Lafleur, B. R. Lutz, E. Fu, P. Yager, A versatile valving toolkit for automating fluidic operations in paper microfluidic devices. *Lab Chip* **15**, 1432–1444 (2015).
32. B. M. Cummins, R. Chinthapatla, F. S. Ligler, G. M. Walker, Time-dependent model for fluid flow in porous materials with multiple pore sizes. *Anal. Chem.* **89**, 4377–4381 (2017).
33. V. V. Doña, C. A. Fossati, F. G. Chirdo, Interference of denaturing and reducing agents on the antigen/antibody interaction. Impact on the performance of quantitative immunoassays in gliadin analysis. *Eur. Food Res. Technol.* **226**, 591–602 (2008).
34. S. Jahanshahi-Anbuhi, P. Chavan, C. Sicard, V. Leung, S. M. Z. Hossain, R. Pelton, J. D. Brennan, C. D. M. Filipe, Creating fast flow channels in paper fluidic devices to control timing of sequential reactions. *Lab Chip* **12**, 5079–5085 (2012).
35. V. R. N. Telis, J. Telis-Romero, H. B. Mazzotti, A. L. Gabas, Viscosity of aqueous carbohydrate solutions at different temperatures and concentrations. *Int. J. Food Prop.* **10**, 185–195 (2007).
36. J. B. Segur, H. E. Oberstar, Viscosity of glycerol and its aqueous solutions. *Ind. Eng. Chem. Res.* **43**, 2117–2120 (1951).